Nuclear Instruments and Methods in Physics Research A 1065 (2024) 169556

Contents lists available at ScienceDirect

Nuclear Inst. and Methods in Physics Research, A

journal homepage: www.elsevier.com/locate/nima

Full Length Article

Performance analysis and testing of LYSO-SiPM X-ray communication receiver

Junxu Mu [a], Yunpeng Liu [a,b,*], Feixu Xiong [a], Junqiu Yin [a], Sheng Lai [a], Kai Miao [a], Xiaobin Tang [a,b,**]

[a] Department of Nuclear Science and Technology, Nanjing University of Aeronautics and Astronautics, Nanjing, 210016, China
[b] Key Laboratory of Nuclear Technology Application and Radiation Protection in Astronautics (Nanjing University of Aeronautics and Astronautics), Ministry of Industry and Information Technology, Nanjing, 210016, China

ARTICLE INFO

Keywords:
X-ray communication
Dead time
Pulse X-ray signal receiver
Active quenching
Photon counting

ABSTRACT

This paper introduces the characteristics of the LYSO-SiPM-based receiver used in X-ray communication (XCOM). The X-ray signal receiving scheme based on a scintillator and photodetector is an important part of the XCOM system. However, the inherent characteristics of the scintillator and photodetector hinder the improvement of the performance of the X-ray signal receiver. Thus, this paper proposes a comprehensive analysis model for modeling the counting statistical characteristics of the LYSO-SiPM-based receiver, and analyzes the effects of the receiver's characteristics on the communication performance of the OOK-modulated XCOM system. Furthermore, the LYSO-SiPM pulse X-ray signal receiver is optimized, and its performance in the XCOM experiment is tested. The experimental results are consistent with the theoretical analysis trend, indicating that the proposed analytical model can be used for XCOM performance analysis and optimization.

1. Introduction

X-ray communication (XCOM) technology is a new communication technology that uses X-rays as a carrier of information transmission [1]. X-ray photons have high energy and strong penetrability, which makes X-ray communication theoretically have larger bandwidth, lower divergence, and higher directionality compared to traditional communication methods. It has good application prospects in the communication of space, spacecraft reentry blackout, and Martian dust environments [2–4], especially that have been proved to be able to penetrate the plasma sheath which the microwave signals are difficult to pass through [3]. The concept of XCOM was first proposed by Gendreau of Goddard Flight Center in the United States [5], and a communication verification experiment was conducted [6]. In our previous study [7], the XCOM system based on a groove-shaped grid-controlled modulated X-ray tube and LYSO-SiPM-based receivers can achieve Mbit/s-level communication capability. XCOM uses intensity modulation direct detection to load and read signals.

As a critical component of the XCOM system, the pulse X-ray receiver determines the quality and upper limit of the communication rate of the system. Our current research uses the LYSO-SiPM-based receiver as an X-ray signal receiver. In this receiver, the $2 \times 2 \times 0.5\ cm^3$ LYSO scintillator receives pulsed X-ray signals and generates optical photon pulses. Subsequently, the optical signals are collected by a SiPM (JARY-TP3050–8 × 8C) [8] to create electrical signals. The structure of the LYSO-SiPM-based receiver is shown in Fig. 1.

X-ray photons interact with the atoms and generate visible light signals after they enter the scintillator. These stages prolong the time of photon generation, transmission, and emission so that the time profiles of the incoming X-ray signal and the outgoing optical signal will no longer coincide [9,10]. SiPM is a novel high-performance semiconductor photodetector composed of multiple avalanche photodiodes (APDs) operating in Geiger mode in parallel [11,12]. APDs operating in Geiger mode can generate macroscopic currents under a single photon, hence they are called single-photon avalanche diodes (SPADs). In Geiger mode, after the avalanche current is generated, the bias voltage needs to be reduced below the breakdown voltage, and this process is called avalanche quenching. Subsequently, it is necessary to increase the bias voltage again to return to the Geiger mode and wait for the next photon incident. During the SPAD quenching-reset period, the device is unable

* Corresponding author. Department of Nuclear Science and Technology, Nanjing University of Aeronautics and Astronautics, Nanjing, 210016, China.
** Corresponding author. Department of Nuclear Science and Technology, Nanjing University of Aeronautics and Astronautics, Nanjing, 210016, China.
E-mail addresses: liuyp@nuaa.edu.cn (Y. Liu), tangxiaobin@nuaa.edu.cn (X. Tang).

https://doi.org/10.1016/j.nima.2024.169556
Received 25 January 2024; Received in revised form 8 June 2024; Accepted 23 June 2024
Available online 28 June 2024

to respond to incoming photons, which is called the dead time. The main ways to achieve avalanche quenching are passive quenching (PQ) mode and active quenching (AQ) mode [13]. The dead time of AQ is constant, whereas, the photons arriving during the dead time can extend their duration in PQ mode.

The nonideal state of the receiver has been studied in optical communication. However, relevant research has not been carried out for X-ray communication. In Ref. [14], the exact expressions for the probability distribution and moments of photocounts in the presence of dead time are derived for active quenching (AQ) and passive quenching (PQ) APDs, and the photocount statistics of an AQ APD receiver with a long dead time are investigated [15].

Huang et al. [16] proposed a novel detection scheme that utilized the information extracted from the counts and arrival times of photons for optimal symbol detection in the presence of nonlinear and random ISI effects to mitigate the performance degradation effectively. In Ref. [17], a method for analyzing the bit error rate (BER) performance of the APD optical receiver is introduced, and the influence of crosstalk and other effects on the performance of the optical receiver is investigated. Establishing the photon counting and BER model of the LYSO-SiPM-based receiver is of great significance to understand its non-ideality effects thoroughly. This approach is very helpful in identifying the most limiting effect for further optimizations and, therefore, is critical to attempt further improvements.

In this work, we establish a mathematical framework to simulate the photon counting behavior and communication capability of the LYSO-SiPM pulse X-ray signal receiver precisely. Based on this model, we provide the exact probability distribution, and mean, to study the effects of dead time, signal intensity, and quenching mode on the counting ability of the LYSO-SiPM-based receiver. We study the BER performance of XCOM links under on–off keying (OOK) modulation. In addition, we build an XCOM experimental platform to test the communication capability of the LYSO-SiPM pulse X-ray signal receiver and compare the theoretical and experimental results.

The remainder of this paper is organized as follows. Section II proposes the nonlinear statistical model of an X-ray signal in the presence. Section III presents the numerical results and analyzes the relationship among data rate, counting performance, and BER. Section IV describes the XCOM experimental testing system model based on the LYSO-SiPM signal receiver and analyzes the experimental results. Finally, Section V provides the concluding remarks.

2. Counting statistics and performance evaluation

2.1. Widening of signal profile caused by LYSO scintillator

According to the luminescence mechanism of scintillators and existing research [18], it is known that after a single X-ray photon is incident, the luminescence intensity of the scintillator will quickly reach its maximum value, and then gradually decrease in a single exponential decay pattern. Its response function can be expressed as:

$$w(t) = (\varepsilon(t) - \varepsilon(t - t_r))\frac{t}{t_r} + \varepsilon(t - t_r)e^{-\frac{t-t_r}{\tau}}, \tag{1}$$

where $\varepsilon(t)$ represents the step function, t_r is the rise time of the scintillation light and τ is the decay time of the scintillator.

The output light intensity of scintillators can be obtained by convolving the X-ray input signal intensity with the scintillator response function, as illustrated in Fig. 2. It is evident that the contour of the output light signal is distorted. The rising edge of the signal undergoes approximately 4 times the decay time before reaching its maximum intensity and maintaining stability. Since signal synchronization during communication relies on the rising edge, the extended rise time can lead to synchronization difficulties. Following the termination of the X-ray signal, the scintillator light response process causes the signal falling edge to decay in a negative exponential form.

The response function of scintillators is determined by their physical processes and cannot be altered. To mitigate the impact of output light signal contour distortion, the X-ray signal waveform of the input scintillator is optimized here. In the initial stage of the signal, in order to shorten the rise time of the light signal output by the scintillator, it is necessary to increase the intensity of the X-ray signal by τ times at the initial moment. In order to reduce the impact of the signal falling edge on subsequent signals, the end time of the signal can be advanced from T to $T - \tau$, which can be expressed as:

$$px(t) = \lambda_X((\varepsilon(t) - \varepsilon(t - 1\ ns))\tau + \varepsilon(t - 1\ ns) - \varepsilon(t - (T - 2\tau))), \tag{2}$$

where λ_X represents normalized X-ray intensity.

The optimized X-ray signal waveform can be convolved with the scintillation response function to obtain the optimized scintillation light waveform as shown in Fig. 3. It can be seen that after optimization, the rising edge of the flicker light waveform is shortened to be the same as t_r (the rise time of the scintillation light after a single X-ray photon is incident), and the falling edge is also reduced, reducing the impact on the next signal.

2.2. Counting statistics of LYSO-SiPM-based receiver

The ideal photon count distribution for SPAD follows the Poisson distribution [19]:

$$p(k,t) = \frac{(\lambda t)^k}{k!}e^{-\lambda t}, \tag{3}$$

where λ is the photon arrival rate, which is proportional to the intensity of the incident X-ray signal, t is the measurement time and k is the number of photons. Due to the existence of dead time (T_d), when SPAD has a photon counting event, its counting process no longer obeys the Poisson distribution.

2.2.1. Renewal process

In this paper, the renewal process model is introduced to calculate the actual photon counting probability distribution. The renewal process

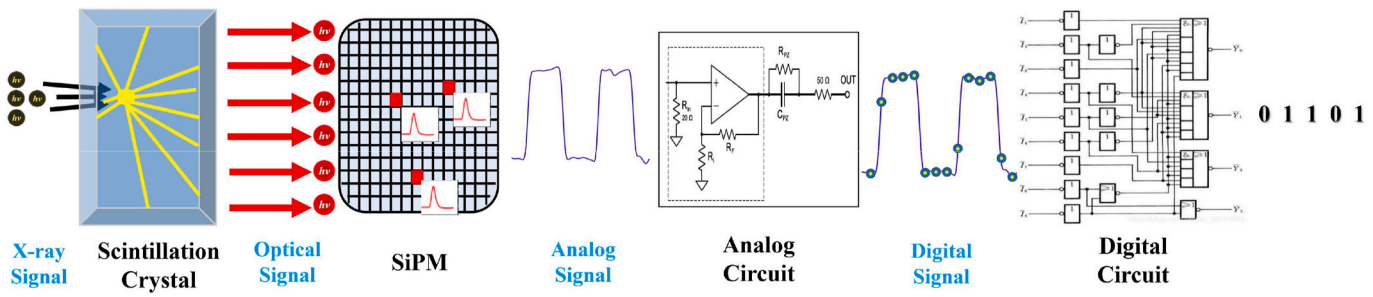

Fig. 1. Schematic of the LYSO -SiPM pulse X-ray signal receiver.

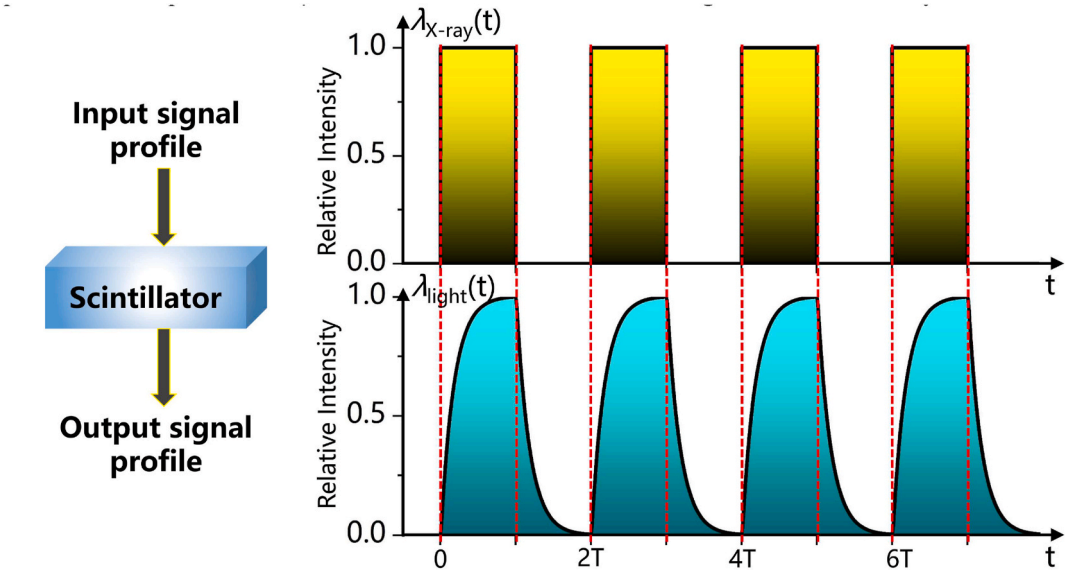

Fig. 2. The optical waveform output by the LYSO scintillator when irradiating square wave X-ray signals.

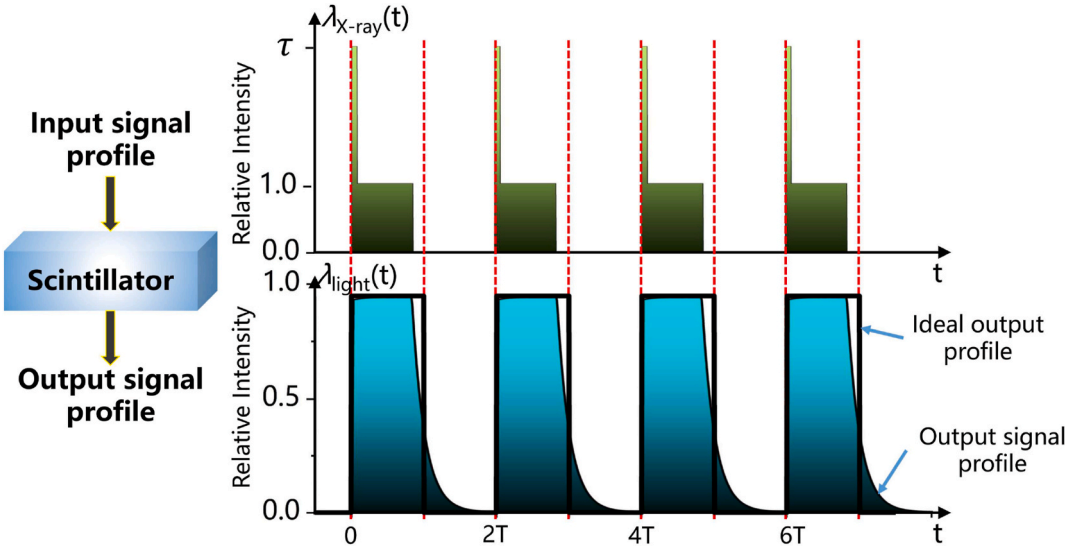

Fig. 3. Optimized optical waveform output by LYSO scintillator.

describes the counting process in which the interval between two adjacent point events corresponds to independent and equally distributed random variables. In the process of counting photons in SPAD, the time interval between two-photon detection conforms to the definition of the update process. Here S_i is used to represent the time interval from the $i-1$ to the i photon count, and its distribution function can be expressed as:

$$F(t) = P\{S_i \le t\} = \int_0^t f(t)dt, \tag{4}$$

where $f(t)$ is the probability density function of $F(t)$.

Define T_k as the total time spent by k renewals, and $N(t)$ as the total number of renewals in the interval $[0,t]$, then the probability distribution $F_k(t)$ of k renewals can be modeled as the k-convolution process of $F(t)$, and the corresponding probability density function $f_k(t)$ of $F_k(t)$ is defined as:

$$F_k(t) = \int_0^t f_k(t)dt. \tag{5}$$

Define $p(k,t)$ as the probability of recording k counts in $[0,t]$:

$$\begin{aligned} p(k,t) &= P\{N(t)=k\} \\ &= P\{N(t)\le k\} - P\{N(t)\le k-1\} \\ &= P\{T_{k+1} > t\} - P\{T_k > t\} \\ &= F_k(t) - F_{k+1}(t) \end{aligned} \tag{6}$$

The above formula shows that the counting distribution $p(k,t)$ at $[0,t]$ can be obtained by solving $F_k(t)$ or $f_k(t)$.

In the actual calculation process, $f(t)$ can be obtained directly. To solve $p(k,t)$ by $f(t)$, we introduce the Laplace transform. Let $\psi(s)$、$\psi_k(s)$、$F_k(s)$ represent the Laplace transform of $f(t)$、$f_k(t)$ and $F_k(t)$, respectively. It has been mentioned before that $f_k(t)$ can be obtained by the k-convolution of $f(t)$, and $F_k(t)$ is the integral of $f_k(t)$, then according to Laplace's integral formula and Laplace's convolution theorem, $F_k(s)$ can be expressed as:

$$F_k(s) = \int_0^\infty F_k(t)e^{-st}dt = \frac{1}{s}\int_0^\infty f_k(t)e^{-st}dt = \frac{1}{s}\psi_k(s) = \frac{\psi(s)^k}{s} \tag{7}$$

The Laplace transform $p(k,s)$ of $p(k,t)$ can be expressed as:

$$p(k,s) = F_k(s) - F_{k+1}(s) = \frac{\psi(s)^k}{s}(1-\psi(s)) \tag{8}$$

By the inverse Laplace transformation of $p(k,s)$, the counting probability distribution $p(k,t)$ can be obtained.

2.2.2. Counting probability distribution of SPAD in active quenching (AQ) mode

In AQ mode, following the detection of a photon and the subsequent output of a count, SPAD experiences a dead time (T_d) during which photons may still reach it, but SPAD will not respond. Assuming that a photon counting event occurs at time $t = 0$, the time interval from $t = 0$ to the occurrence of the next counting event comprises two distinct phases: (1) SPAD cannot respond to photons during $[0, T_d]$ time. (2) After T_d, photons arrive and are counted at time t. Since the process of photons reaching the SPAD occurs continuously and independently at a constant average rate, the probability of phase (2) can be calculated from a negative exponential distribution. So, the probability density function $f(t)$ for the time between two counting events can be expressed as:

$$f(t) = (\varepsilon(t) - \varepsilon(t-T_d)) * 0 + \varepsilon(t-T_d)\lambda e^{-\lambda(t-T_d)}. \tag{9}$$

Therefore, SPAD is idle at time $t = 0$, and its counting probability $p_{AQ}(k,t)$ can be expressed as follows: a photon counting event occurs at the time t_1, and the $k-1$ counting renewal process matching formula (9) occurs at the time (t_1, t), and its mathematical expression can be written as:

$$p_{AQ}(k,t) = \lambda e^{-\lambda t} \otimes p_{A,rp}(k-1,t), \tag{10}$$

where $\otimes$ represents the convolution process and $p_{A,rp}(k-1,t)$ represents the photon counting renewal process in AQ mode.

According to equation (7), the Laplace transform of $f(t)$ can be obtained as:

$$\psi(s) = \int_0^\infty f(t)e^{-st}dt = \int_{T_d}^\infty \lambda e^{-\lambda(t-T_d)}e^{-st}dt = \frac{\lambda}{s+\lambda}e^{-sT_d} \tag{11}$$

Combined with formulas (8) and (10), the Laplace transform of AQ-SPAD counting probability $p_{AQ}(k,t)$ under can be expressed as:

$$\begin{aligned} P_{AQ}(k,s) &= \int_0^\infty p_{AQ}(k,t)e^{-st}dt \\ &= \int_0^\infty \left(\lambda e^{-\lambda t} \otimes p_{A,rp}(k-1,t)\right)e^{-st}dt \\ &= \frac{\lambda}{s+\lambda} * \left(\frac{\psi(s)^{k-1}}{s}(1-\psi(s))\right) \end{aligned} \tag{12}$$

Bringing in formula (11), we get the Laplace transform of $p_{AQ}(k,t)$:

$$P_{AQ}(k,s) = \frac{\lambda}{s(s+\lambda)}\left(\left(\frac{\lambda e^{-sT_d}}{s+\lambda}\right)^{k-1} - \left(\frac{\lambda e^{-sT_d}}{s+\lambda}\right)^k\right) \tag{13}$$

By applying the Laplace inverse transformation to equation (13), the total counting probability of AQ-SPAD in an idle state can be obtained (a detailed derivation process can be found in Appendix A):

$$\begin{aligned} p_{AQ}(k,t) = \varepsilon(t-kT_d)&\left(\sum_{i=0}^{k}\frac{(\lambda(t-kT_d))^i}{i!}e^{(-\lambda(t-kT_d))} - 1\right) - \varepsilon(t \\ &- (k-1)T_d)\left(\sum_{i=0}^{k-1}\frac{(\lambda(t-(k-1)T_d))^i}{i!}e^{(-\lambda(t-(k-1)T_d))} - 1\right) \end{aligned} \tag{14}$$

It can be concluded that the total counting probability of AQ-SPAD during $[0, T]$ is:

$$p_{AQ}(k,T) = \begin{cases} \sum_{i=0}^{k} X(i,\lambda(T-kT_d)) - \sum_{i=0}^{k-1} X(i,\lambda(T-(k-1)T_d)), k < k_{max} \\ 1 - \sum_{i=0}^{k-1} X(i,\lambda(T-(k-1)T_d)), k = k_{max} \end{cases} \tag{15}$$

where $X(a,b) = b^a e^{-b}/a!$, $k_{max} = \lfloor T/T_d \rfloor + 1$, $\lfloor x \rfloor$ represents rounding down.

2.2.3. Counting probability distribution of SPAD in PQ mode

In passive quenching (PQ) mode, following the detection of a photon and the subsequent output of a pulse, the SPAD also experiences a dead time of T_d. However, its renewal process is different from the AQ mode. If a photon arrives during the dead time, SPAD will not have a new counting, but the newly arrived photon will prolong the time when SPAD cannot work in AQ mode.

The statistical properties of SPAD photon counts are obtained by constructing a counting renewal process in PQ mode, which is similar to AQ mode. Here the renewal function $M(t)$ and renewal density $m(t)$ are introduced to calculate the probability distribution function $f_k(t)$ in PQ mode. The renewal function is the average number of renewals of the renewal process in $(0,t)$, which can be expressed as:

$$M(t) = EN(t) = \sum_{k=1}^{\infty} F_k(t) \tag{16}$$

The renewal density is the derivative of the renewal function, and its mathematical meaning can be interpreted as the average renewal rate of the renewal process in $(0,t)$. By definition, $m(t)$ can be expressed as:

$$m(t) = M'(t) = \sum_{k=1}^{\infty} f_k(t) \tag{17}$$

For the renewal process of the PQ-SPAD, the average renewal rate of the count can be described as after the count occurs at $t = 0$, no photon counting event will occur in $(0, T_d)$. After T_d, no photon arrives within $(t - T_d, t)$, and a photon arrival event occurs at time t. From this, a mathematical expression for the renewal density $m(t)$ can be constructed:

$$m(t) = (\varepsilon(t) - \varepsilon(t-T_d)) * 0 + \varepsilon(t-T_d)e^{-\lambda(t-(t-T_d))}\lambda = \varepsilon(t-T_d)\lambda e^{-\lambda T_d} \tag{18}$$

By combining equations (17) and (18), we can obtain:

$$\sum_{k=1}^{\infty} f_k(t) = \varepsilon(t-T_d)\lambda e^{-\lambda T_d} \tag{19}$$

To calculate $f(t)$, the Laplace transform is also introduced here. By applying the Laplace transform to equation (19) and using Laplace integral theorem, we can obtain:

$$\sum_{k=1}^{\infty} \psi_{k,PQ}(s) = \sum_{k=1}^{\infty} \psi_{PQ}(s)^k = \frac{\lambda e^{-(s+\lambda)T_d}}{s} \tag{20}$$

By replacing and simplifying the summation term in the equation using formula (21), we can obtain formula (22):

$$\sum_{i=0}^{\infty}\binom{k+i-1}{i}x^i = \frac{1}{(1-x)^k}, -1 < x < 1 \tag{21}$$

$$\psi_{PQ}(s) = \frac{\lambda e^{-(s+\lambda)T_d}}{s+\lambda e^{-(s+\lambda)T_d}} = \frac{\lambda e^{-(s+\lambda)T_d}}{s\left(1+\frac{\lambda}{s}e^{-(s+\lambda)T_d}\right)} \tag{22}$$

According to formula (21), replace and simplify the parentheses in the denominator of the above formula again, and equation (22) becomes:

$$\psi_{PQ}(s) = \frac{\lambda e^{-(s+\lambda)T_d}}{s} \sum_{i=0}^{\infty} \left(-\frac{\lambda}{s} e^{-(s+\lambda)T_d} \right)^i = -\sum_{i=1}^{\infty} (-\lambda)^i \frac{e^{-(s+\lambda)iT_d}}{s^i} \tag{23}$$

By calculating the Laplace inverse transform of the above formula, the probability density function of the interval time between two counting events of PQ-SPAD can be obtained:

$$f(t) = \lambda e^{-\lambda t} \sum_{i=1}^{k_{max}-1} X(i-1, \lambda(iT_d - t)) \tag{24}$$

Similar to AQ mode, here we also construct the Laplace transform for $p(k,t)$ in PQ mode:

$$P_{PQ}(k,s) = \frac{\lambda}{s+\lambda}(F_{k-1}(s) - F_k(s)) \tag{25}$$

Substituting formula (23):

$$P_{PQ}(k,s) = \frac{\lambda}{s(s+\lambda)} \left(\frac{\lambda e^{-(s+\lambda)T_d}}{s+\lambda e^{-(s+\lambda)T_d}} \right)^{k-1} \left(1 - \frac{\lambda e^{-(s+\lambda)T_d}}{s+\lambda e^{-(s+\lambda)T_d}} \right) \tag{26}$$

By calculating the inverse Laplace transform of equation (26), the total counting probability of SPAD in the idle state can be obtained (see Appendix B for detailed derivation):

$$p_{PQ}(k,t) = \sum_{i=k}^{k_{max}} \binom{i-1}{i-k} (-1)^k e^{-\lambda t} \left(1 - \sum_{r=0}^{i-1} \mathrm{X}(r, \lambda((i-1)\,T_d - t)) \right) \tag{27}$$

It can be obtained that the total counting probability of PQ-SPAD during $[0,T]$ is:

$$p_{PQ}(k,T) = e^{-\lambda T} \sum_{i=k}^{k_{max}} \binom{i-1}{i-k} (-1)^k \left(1 - \sum_{r=0}^{i-1} \mathrm{X}(r, \lambda((i-1)T_d - T)) \right) \tag{28}$$

2.2.4. Counting characteristic analysis

The probability distributions of SPAD counting models in AQ mode and PQ mode obtained through equations (15) and (28) are plotted in Fig. 4 with $T = 5\ \mu s$ and $\lambda = 9 \times 10^6$ photon/s. It can be seen that if the dead time doesn't exist, the photon counting of SPAD follows a Poisson distribution. When $T_d > 0$, the SPAD counts in both AQ and PQ modes don't follow the Poisson distribution, and the larger the dead time, the more severe the deviation from the Poisson distribution. As the T_d increases, the average counting of SPAD gradually decreases. The main reason is that the dead time leads to a decrease in effective counting time, resulting in a gradual decrease in the average counting.

From Fig. 4, it can also be seen that under the same conditions, the average counting of AQ mode is higher than PQ mode. To provide a more intuitive comparison, Fig. 5 shows the counting probability distribution of SPAD in AQ mode and PQ mode under the same conditions. It is not difficult to see that the highest counting probability of AQ-SPAD occurs at $k = 16$, and k has a probability of more than 90% falling within 13–18. Under the same conditions, the highest counting probability of PQ mode occurs at k = 8, with only a 2% probability that $k \geq 12$. The main reason for this phenomenon is that the blocking time (i.e. the time when SPAD cannot work) of SPAD in AQ mode is constant, while the blocking time of PQ-SPAD will extend with the arrival of new photons during quenching. Therefore, the effective counting time of PQ-SPAD is inevitably smaller than that of AQ-SPAD, causing its counting probability to shift towards a decrease in k.

Fig. 6 shows the average counting values at different photon incidence rates. It can be seen that under ideal conditions, the photon counting distribution follows a Poisson distribution, and its mean is proportional to the photon incidence rate. In reality, due to the existence of dead time, its counting probability distribution deviates from the Poisson distribution, and the degree of deviation gradually increases

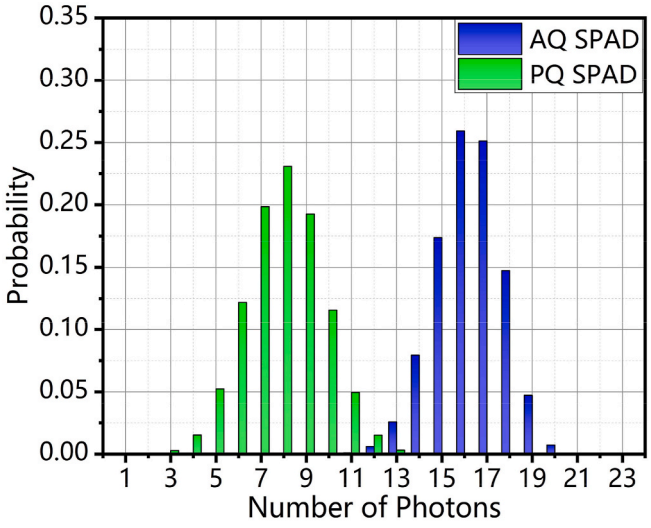

Fig. 5. Comparison of SPAD counting distribution between AQ and PQ modes.

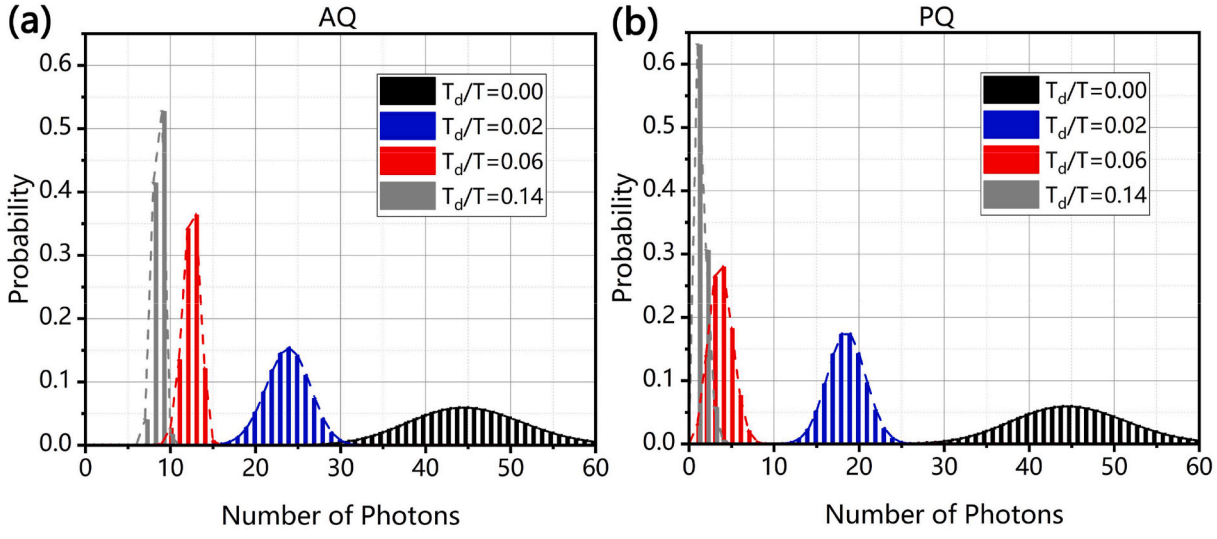

Fig. 4. Probability distribution of AQ (a) and PQ (b) SPAD counting models.

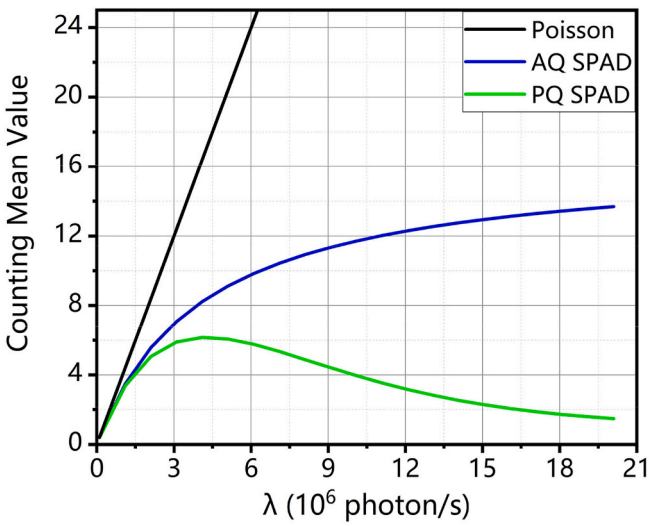

Fig. 6. The variation of counting mean value with photon incidence rate under different counting models.

with the increase of the photon incidence rate. For AQ-SPAD, the average photon counting gradually increases with increasing photon rate, but the growth rate gradually decreases. As the photon rate increases, the average counting of PQ-SPAD increases to the maximum value and then gradually decreases. This is because as the photon incidence rate increases, the blocking time of PQ-SPAD will also be prolonged, leading to SPAD saturation and making photon counting impossible.

2.3. Counting probability distribution in the presence of ISI

The counting probability distribution for an idle SPAD has been deduced. In a signal period, the arrival of one photon produces dead time that affects the counting of other photons. Between adjacent signal periods, the dead time of the previous signal period may still exist at the beginning of the next signal period, so that the time available for photon counting in the next signal period is reduced, resulting in a change in the probability distribution of photon counting in the next signal period, which is called intersymbol interference (ISI), as shown in Fig. 7.

It can be seen from Fig. 7 that at time t_s, the last photon counting occurs, and the SPAD cannot work for some time thereafter until the time t_B, when the SPAD returns to active state. The t_B maybe within this signal period or fall into the next signal period. If t_B falls into the next signal period, the time available for photon counting changes from T to $-t_B$, changing the counting probability distribution in the next signal period from $p(k,T)$ to $p(k,T-t_B)$.

To analyze the impact of ISI, the average time $E(t_s)$ of the last count within a signal period and the average blocking time $E(T_d)$ are calculated. If $t_B<0$, means it is within a current signal period, and the next signal period can start working from time 0. Therefore, t_B can be written as:

$$t_B = max\{0, E(t_s)+E(T_d)-T\} \tag{29}$$

2.3.1. Blocking time

In AQ mode, the blocking time $T_{d,AQ}$ is equal to T_d. In PQ mode, the blocking time is a probability distribution of time. Since the probability density function of the photon counting in PQ mode can be expressed as the convolution of the photon counting process in SPAD blocking and idle states, according to the Laplace convolution theorem, the Laplace transform of the blocking time $T_{d,PQ}$ in PQ mode can be expressed as:

$$T_{d,PQ}(s) = \frac{\psi_{PQ}(s)}{\frac{\lambda}{s+\lambda}} = \frac{e^{-(s+\lambda)T_d}(s+\lambda)}{s+\lambda e^{-(s+\lambda)T_d}}. \tag{30}$$

The probability density function can be obtained by the inverse Laplace transformation:

$$T_{d,PQ}(t) = e^{-\lambda T_d}\delta(t-T_d) - \lambda e^{-\lambda t}\sum_{r=1}^{2}\left((-1)^r \sum_{i=r}^{k_{max}-1} \mathrm{X}(i-1,\lambda(iT_d-t))\right) \tag{31}$$

where $\delta(t)$ is the unit impulse function. The expectation of $T_{d,PQ}(t)$ can be obtained through (32):

$$E(T_{d,PQ}) = \int_0^{+\infty} tT_{d,PQ}(t)dt \tag{32}$$

2.3.2. Average time of the last counting

Let $t_s(k,t)$ represent the time when the last photon counting occurred within a signal period. As discussed in the previous section, $t_s(k,t)$ can be expressed as SPAD in an idle state, where a photon counting event occurs at the time t_1, and a k-1 count renewal process occurs within time (t_1,t), so its Laplace transform is:

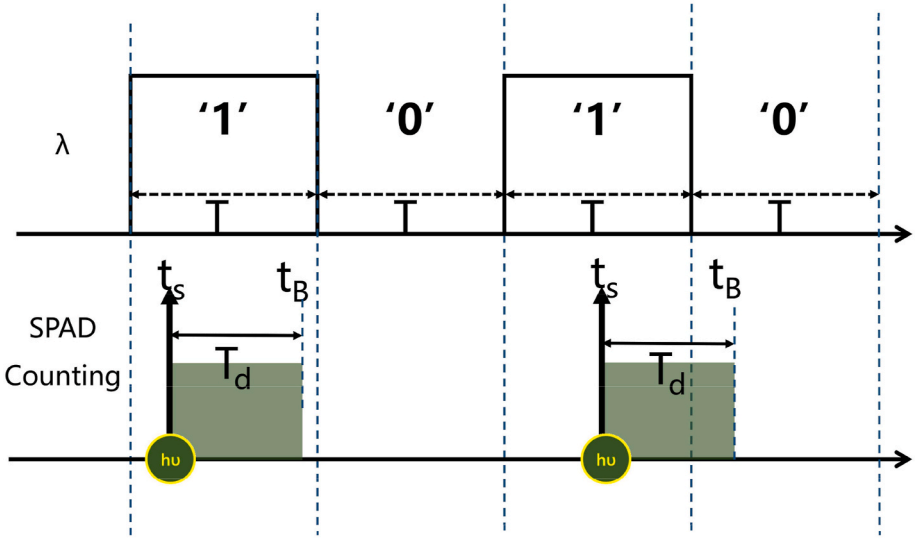

Fig. 7. ISI caused by dead time.

$$t_s(k,s) = \frac{\lambda}{s+\lambda}\psi_{k-1}(s) = \frac{\lambda\psi(s)^{k-1}}{s+\lambda} \tag{33}$$

Substitute the $\psi_{AQ}(s)$ and $\psi_{PQ}(s)$ obtained in the previous section and calculate the Laplace inverse transformation to obtain the time $t_{s,AQ}(k,t)$ and $t_{s,PQ}(k,t)$ in AQ and PQ modes:

$$t_{s,AQ}(k,t) = \varepsilon(t-(k-1)T_d)\frac{\lambda^k(t-(k-1)T_d)^{k-1}}{(k-1)!}e^{-\lambda(t-(k-1)T_d)} \tag{34}$$

$$t_{s,PQ}(k,t) = \sum_{i=k-1}^{k_{max}-1}\binom{i-1}{k-2}(-1)^{k-1}\lambda e^{-\lambda t}\left(1-\sum_{r=0}^{i-1}\mathrm{X}(r,(\lambda(iT_d-t)))\right) \tag{35}$$

The last counting time of 0-k counts within a signal period can be obtained from equations (34) and (35), and by substituting it into equation (36), the average time $E(t_s)$ of the last count per unit period can be obtained.

$$E(t_s) = \sum_{k=0}^{kmax} p(k,T) * \int_0^T t * \frac{t_s(k,t)}{\int_0^T t_s(k,t)dt}dt \tag{36}$$

3. Communication performance evaluation

3.1. BER model in OOK modulation

X-ray communication technology currently uses intensity modulation direct detection (IM/DD) to load signals, with the simplest being on–off keying (OOK) modulation. OOK modulation sends binary information through the presence or absence of optical pulses: when the signal source outputs a binary signal "1″, optical pulses are sent; when the binary signal "0″ is output, no optical pulses are sent. Similarly, the signal receiving end makes judgments based on the intensity of the received optical pulses. Those above the intensity threshold are considered as binary signal "1″, while those below the threshold are considered as binary signal "0".

$$P_\xi(k) = \frac{1}{2}p\big(k,\lambda_\xi,T_d,(T-t_B(\lambda_1))\big) + \frac{1}{2}p\big(k,\lambda_\xi,T_d,(T-t_B(\lambda_0))\big), \tag{37}$$

where the ξ represents a "0″ or "1". The mean μ_ξ and variance ${\sigma_\xi}^2$ can be calculated using the following formula:

$$\mu_\xi = \sum_{k=0}^{k_{max}} P_\xi(k) * k \tag{38}$$

$${\sigma_\xi}^2 = \sum_{k=0}^{k_{max}} P_\xi(k) * \big(k-\mu_\xi\big)^2 \tag{39}$$

This study used SiPM to receive scintillation photons generated by LYSO scintillators. SiPM consists of N independent working SPADs. According to the central limit theorem [20], when the sample size N is large enough, the sum of N independent and identically distributed random variables approximately follows a normal distribution $X \sim N(\mu_N,\sigma_N^2)$, where

$$\mu_N = \sum_{j=1}^{N}\mu_j = N\mu_\xi, \tag{40}$$

$$\sigma_N^2 = \sum_{j=1}^{N}\sigma_j^2 = N{\sigma_\xi}^2, \tag{41}$$

The key indicator to measure the reliability of a communication system is the bit error rate (BER), which can be represented by equation (42):

$$BER = \frac{1}{2}(P(0|1)+P(1|0)) = \frac{1}{2}\sum_{k=0}^{K_{th}}p_1(k) + \frac{1}{2}\sum_{k=K_{th}}^{k_{max}}p_0(k) \tag{42}$$

where K_{th} is the decision threshold.

In OOK modulation, it is generally assumed that the probability of the occurrence of "0″ and "1″ signals is equal [21]. According to the maximum likelihood criterion, the optimal decision threshold K_{th} for OOK can be obtained by the intersection of the probability density distributions of the "0″ signal and the "1″ signal, which can be expressed as:

$$\frac{1}{\sqrt{2\pi{\sigma_{N,0}}^2}}exp\left(-\frac{(K_{th}-\mu_{N,0})^2}{2{\sigma_{N,0}}^2}\right) = \frac{1}{\sqrt{2\pi{\sigma_{N,1}}^2}}exp\left(-\frac{(K_{th}-\mu_{N,1})^2}{2{\sigma_{N,1}}^2}\right), \tag{43}$$

where $\mu_{N,0}$、$\mu_{N,1}$、${\sigma_{N,0}}^2$、${\sigma_{N,1}}^2$ represent the mean and variance of the "0″ signal and the "1″ signal, respectively. By solving this formula, the K_{th} can be obtained as follows:

$$K_{th} = \frac{\frac{\mu_{N,0}}{{\sigma_{N,0}}^2} - \frac{\mu_{N,1}}{{\sigma_{N,1}}^2} + \sqrt{\left(\frac{\mu_{N,0}}{{\sigma_{N,0}}^2}-\frac{\mu_{N,1}}{{\sigma_{N,1}}^2}\right)^2 - \left(\frac{1}{{\sigma_{N,0}}^2}-\frac{1}{{\sigma_{N,1}}^2}\right)\left(\frac{{\mu_{N,0}}^2}{{\sigma_{N,0}}^2}-\frac{{\mu_{N,1}}^2}{{\sigma_{N,1}}^2}+ln\frac{{\sigma_{N,0}}^2}{{\sigma_{N,1}}^2}\right)}}{\frac{1}{{\sigma_{N,0}}^2}-\frac{1}{{\sigma_{N,1}}^2}} \tag{44}$$

3.2. Communication performance analysis

The BER of AQ-SiPM (a) and PQ-SiPM (b) obtained from formula (42) as a function of data rate and dead time are shown in Fig. 8, where λ_1 and λ_0 are 10×10^6 photon/s, 1×10^6 photon/s respectively. At the same photon incidence rate, the BER of both modes will gradually increase with the increase in data rate and dead time, the reason is that the increase of dead time and communication rate will cause a decrease in the effective counting time of SiPM per period, resulting in a decrease in the photon counting difference between the "1″ signal and the "0″ signal, leading to an increase in BER.

In addition, comparing the two working modes, it can be found that under the same conditions, the BER of the AQ mode is always lower than that of the PQ mode, which is consistent with the results discussed in the previous section. At the same data rate, the BER of the PQ mode shows a significant upward trend with increasing dead time, while the error rate of the AQ mode shows relatively insignificant changes with dead time. The main reason is that under the same conditions, the blocking time of AQ-SiPM is fixed and directly controlled by external circuits, while the blocking time of AQ-SiPM significantly increases with the increase of dead time, resulting in a significant decrease in its signal discrimination.

The variation of BER of AQ-SiPM (a) and PQ-SiPM (b) with λ_1 and λ_0 is shown in Fig. 9, where the data rate is 1.0 Mbit/s and T_d is 100 ns. It is not difficult to see from the figure that as the background light intensity increases, the BER of SiPM will increase in both operating modes. As the intensity of the "1″ signal increases, the BER of AQ-SiPM will gradually

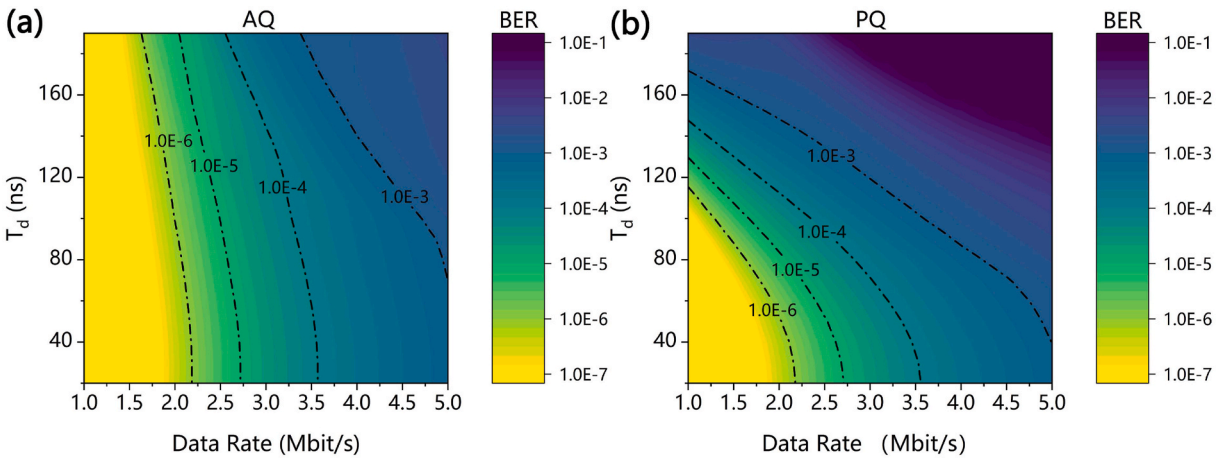

Fig. 8. BER versus different dead time and data rate in AQ (a) and PQ (b) modes.

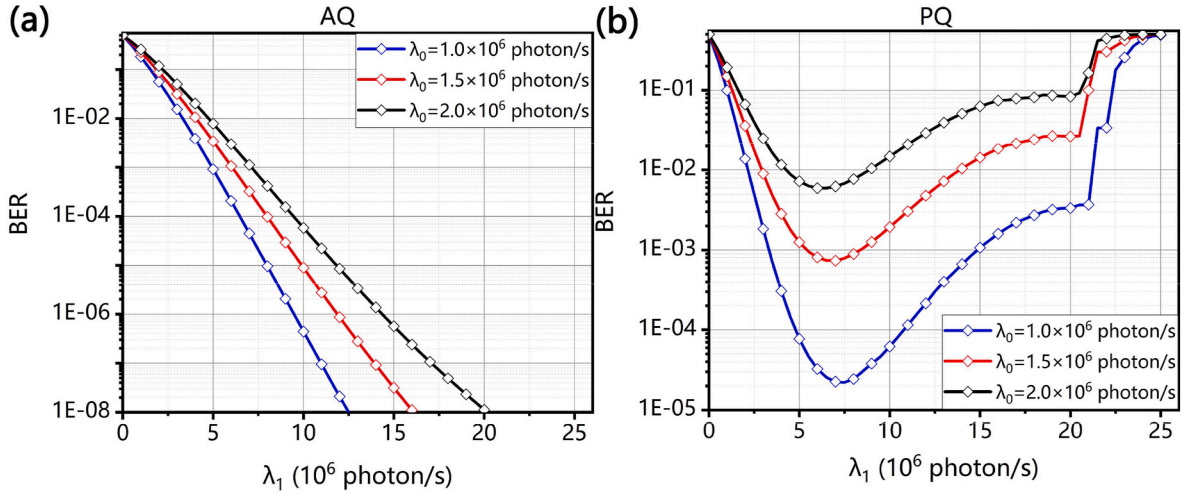

Fig. 9. BER versus different signal intensity in AQ (a) and PQ (b) counting modes.

decrease. In PQ mode, BER first decreases and then increases with the increase of "1″ signal intensity. The main reason is that the increase in signal intensity not only increases the probability of counting per unit time but also increases the blocking time of PQ mode, reducing the effective counting time of each period. Therefore, for PQ-SiPM, blindly increasing the signal light intensity does not always improve communication performance.

4. Experimental test and results

Our previous research has developed the PQ-LYSO-SiPM pulse X-ray receiver [7]. By adding an active quenching module, the existing X-ray receiver has been improved, and an AQ-LYSO-SiPM pulse X-ray signal receiver has been obtained. The active quenching module is mainly composed of a bias control module based on FPGA and a switch circuit based on an MOS transistor.

An XCOM performance test system is built using the developed LYSO-SiPM pulse X-ray signal receiver and the laboratory's existing grid-controlled modulated X-ray tube (GMXT) [22], as shown in Fig. 10. The pseudo-random code is generated by the upper computer and its signal waveform is optimized according to the method in section 2.1. The optimized signal waveform was amplified by the power amplifier (AIGTEK4315) and loaded on the grid of the X-ray tube. The grid's electric field can control the electron beam switch bombarding the anode target to realize the generation of modulated X-ray signals. After the transmission in the air channel, the pulse X-ray signal reaches the pulse X-ray receiver. The signal processing module of the pulse X-ray receiver restores the signal and transmits it to the lower computer for analysis.

During the BER test, the anode voltage of GMXT was set to 45 kV, and the filament current was set to 1.5 A. The pseudo-random code PRBS7 was used to test the BER, and the signal received by the receiver was demodulated offline by the lower computer.

The change of experimental BER with dead time in AQ mode is shown in Fig. 11(a). The experimental results indicate that in AQ mode, the increase in T_d and data rate leads to an increase in the BER of the experimental, which is consistent with the results of numerical analysis. The change of BER with data rate and quenching mode at $T_d = 150$ ns was tested and compared with the analytical value. The results are shown in Fig. 11(b). In both quenching modes, the BER of the X-ray signal receiver increases with the increase in data rate. In addition, under the same data rate, comparing the two quenching modes, it can be found that AQ mode can achieve better communication performance than PQ mode. At the BER of 1.0×10^{-3}, the data rate of the AQ-LYSO-SiPM X-ray signal receiver can reach 2.8 Mbit/s, which is 1.0 Mbit/s higher than PQ-LYSO-SiPM.

However, compared with the calculation results, the BER of the experimental results under the same conditions is higher. On the one hand, the experimental process uses a fixed threshold detection signal, which is different from the optimal communication performance based

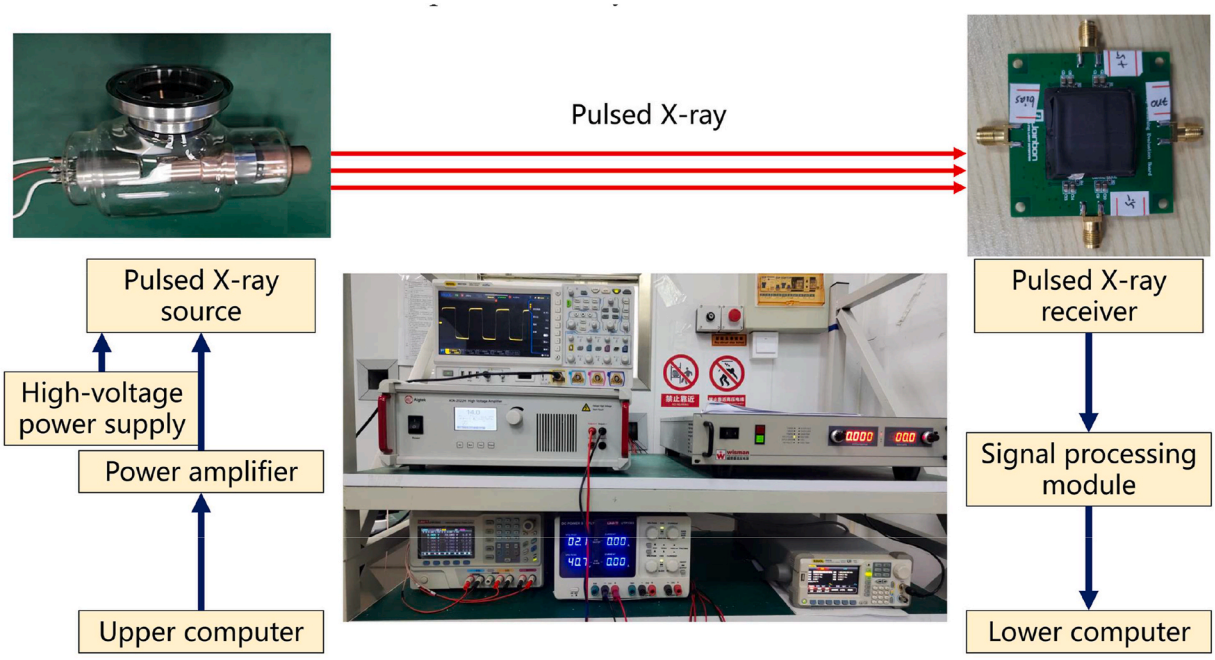

Fig. 10. Experimental setup of XCOM performance test system.

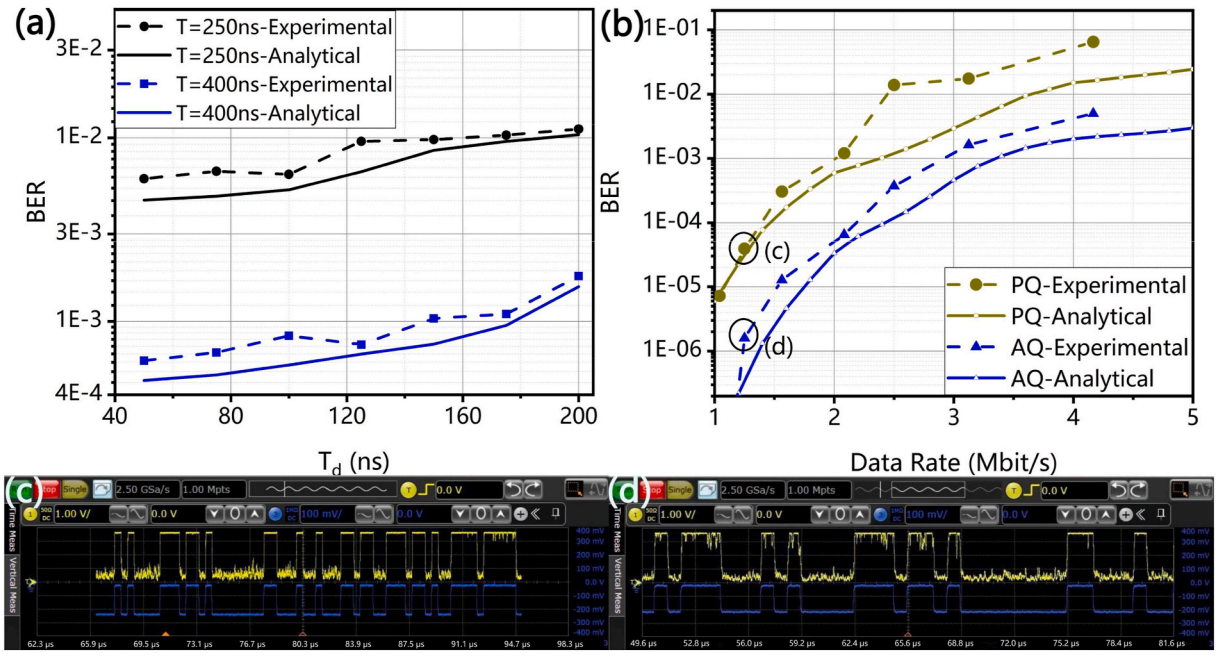

Fig. 11. Experimental (dotted curves) and analytical (solid curves) BER results of an LYSO-SiPM-based receiver for dead time in AQ mode (a), data rate and quenching mode (b), and the snapshots of the analog signal directly from the oscilloscope in PQ mode (c) and AQ mode (d).

on the maximum likelihood estimation shown by the theoretical calculation results. On the other hand, due to the limitations of device performance, the signal waveform emitted by the pulse X-ray source gradually distorts with the increase of data rate, resulting in a certain degree of jitter in the amplitude of the X-ray signal. In the future, we will optimize the experimental parameter settings of the duty period according to the theoretical calculation results to improve the communication performance further.

5. Conclusions

We study the BER performance modeling and analysis based on the LYSO-SiPM pulse X-ray signal receiver and experimentally verify the performance of this receiver. This model covers significant nonideal effects that allow more insights into the overall performance and enable the evaluation of the contribution to the BER. The influence of the dead time, signal intensity, and quenching mode on the counting statistics of the detector was studied, and the expressions of photon counting probability distribution and BER performance of the LYSO-SiPM-based receiver were provided. Due to the influence of dead time, the number

of photons detected by the LYSO-SiPM pulse X-ray receiver over a fixed time interval does not follow a Poisson distribution. The distorted counting statistics result in a higher BER. For AQ-LYSO-SiPM, in order to maintain communication performance at higher data rates, it is necessary to increase the X-ray signal intensity. However, blindly increasing signal intensity in PQ mode cannot always reduce the BER. Under the same conditions, the performance of AQ-LYSO-SiPM is significantly better than that of PQ-LYSO-SiPM. Theoretically, when the background and signal photon rates are 0.7×10^6 photon/s and 7.1×10^6 photon/s, respectively, with a T_d of 150ns and a target BER of 1.0×10^{-3}, AQ-LYSO-SiPM can achieve a data rate of 3.2 Mbit/s, while the data rate of PQ-LYSO-SiPM is only 2.1 Mbit/s. The results of X-ray communication experiments are consistent with the trend of theoretical analysis, indicating that the BER analysis model in this paper can be used for the analysis and performance optimization of LYSO-SiPM pulse X-ray signal receivers.

CRediT authorship contribution statement

Junxu Mu: Writing – original draft, Methodology, Investigation, Data curation. **Yunpeng Liu:** Writing – review & editing, Supervision, Funding acquisition. **Feixu Xiong:** Writing – review & editing, Conceptualization. **Junqiu Yin:** Writing – review & editing, Validation. **Sheng Lai:** Writing – review & editing, Formal analysis. **Kai Miao:** Writing – review & editing, Validation. **Xiaobin Tang:** Writing – review & editing, Supervision, Funding acquisition.

Declaration of competing interest

The authors declare that they have no known competing financial interests or personal relationships that could have appeared to influence the work reported in this paper.

Data availability

Data will be made available on request.

Acknowledgments

This work was supported by the National Natural Science Foundation of China (Grant No. 12375256) and the Fundamental Research Funds for the Central Universities (Grant No. NT2023012).

Appendix A

Equation (13) can be written as:

$$P(k,s) = \frac{\lambda}{s(s+\lambda)}\left(\left(\frac{\lambda e^{-sT_d}}{s+\lambda}\right)^{k-1} - \left(\frac{\lambda e^{-sT_d}}{s+\lambda}\right)^{k}\right) = \frac{\lambda^k e^{-s(k-1)T_d}}{s^{k+1}\left(1+\frac{\lambda}{s}\right)^k} - \frac{\lambda^{k+1} e^{-skT_d}}{s^{k+2}\left(1+\frac{\lambda}{s}\right)^{k+1}} \tag{A 1}$$

The parentheses in the denominator of the above formula are replaced and simplified according to formula (21), which is converted to:

$$P(k,s) = \sum_{i=0}^{\infty}\binom{k+i-1}{i}(-1)^i\frac{\lambda^{k+i}e^{-s(k-1)T_d}}{s^{k+i+1}} - \sum_{i=0}^{\infty}\binom{k+i}{i}(-1)^i\frac{\lambda^{k+i+1}e^{-skT_d}}{s^{k+i+2}} \tag{A 2}$$

By applying Laplace inverse transformation to the above equation, we can obtain:

$$p(k,t) = \sum_{i=0}^{\infty}\binom{k-1+i}{i}(-1)^i\lambda^{k+i}\varepsilon(t-(k-1)T_d)\frac{(t-(k-1)T_d)^{k+i}}{(k+i)!} - \sum_{i=0}^{\infty}\binom{k+i}{i}(-1)^i\lambda^{k+i+1}\varepsilon(t-kT_d)\frac{(t-kT_d)^{k+i+1}}{(k+i+1)!} \tag{A 3}$$

Substitute the combination numbers in equation (A.3) with equation (A.4), and simplify it to obtain equation (A.5):

$$\binom{k+i}{i} = \sum_{n=1}^{k+1}(-1)^{n-1}\binom{i+k+1}{i+n} \tag{A 4}$$

$$p(k,t) = \sum_{i=0}^{\infty}\sum_{n=1}^{k}\varepsilon(t-(k-1)T_d)(-1)^{k-1+n}\frac{(-\lambda(t-(k-1)T_d))^{k+i}}{(i+n)!(k-n)!}\Bigg) - \sum_{i=0}^{\infty}\sum_{n=1}^{k+1}(-1)^{k+n}\varepsilon(t-kT_d)\frac{(-\lambda(t-kT_d))^{k+i+1}}{(i+n)!(k+1-n)!} \tag{A 5}$$

By simplifying the above formula, we get:

$$p(k,t) = \sum_{n=1}^{k+1}\varepsilon(t-kT_d)\frac{(\lambda(t-kT_d))^{k+1-n}}{(k+1-n)!}\left(\sum_{i=n}^{\infty}\frac{(-\lambda(t-kT_d))^i}{i!}\right) - \sum_{n=1}^{k}\varepsilon(t-(k-1)T_d)\frac{(\lambda(t-(k-1)T_d))^{k-n}}{(k-n)!}\left(\sum_{i=n}^{\infty}\frac{(-\lambda(t-(k-1)T_d))^i}{i!}\right) \tag{A 6}$$

The right parentheses in the above equation are replaced by formula (A.7) and simplified, and equation (A.8) can be obtained after simplification:

$$e^x = \sum_{i=0}^{\infty}\frac{x^i}{i!} \tag{A 7}$$

$$p(k,t) = \varepsilon(t-kT_d)\left(\sum_{i=0}^{k}\frac{(\lambda(t-kT_d))^i}{i!}e^{(-\lambda(t-kT_d))} - 1\right) - \varepsilon(t-(k-1)T_d)\left(\sum_{i=0}^{k-1}\frac{(\lambda(t-(k-1)T_d))^i}{i!}e^{(-\lambda(t-(k-1)T_d))} - 1\right) \tag{A 8}$$

Appendix B

Equation (26) can be written as:

$$P(k,s)=\frac{\lambda}{s(s+\lambda)}\frac{\left(\frac{\lambda}{s}e^{-(s+\lambda)T_d}\right)^{k-1}}{\left(1+\frac{\lambda}{s}e^{-(s+\lambda)T_d}\right)^{k}} \tag{B 1}$$

Here, formula (21) is used to replace the power term in the denominator of the above formula, we get:

$$P(k,s)=\sum_{i=0}^{\infty}\binom{k+i-1}{i}(-1)^i\lambda^{i+k}\frac{e^{-(s+\lambda)(i+k-1)T_d}}{s^{i+k+1}}\frac{1}{1+\frac{\lambda}{s}} \tag{B 2}$$

Substitute the $(1+\lambda/s)$ again using formula (21):

$$P(k,s)=\sum_{i=0}^{\infty}\binom{k+i-1}{i}\sum_{r=0}^{\infty}(-1)^{r+i}(\lambda)^{r+i+k}\frac{e^{-(s+\lambda)(i+k-1)T_d}}{s^{i+k+1+r}} \tag{B 3}$$

Taking the inverse Laplace transform of this formula:

$$p(k,t)=\sum_{i=k-1}^{\infty}\binom{i}{i-k+1}\varepsilon(t-iT_d)e^{-iT_d\lambda}(-1)^k\sum_{w=i+1}^{\infty}\frac{(-\lambda(t-iT_d))^w}{w!} \tag{B 4}$$

Replace the infinite series term at the end of the formula with formula (A.7), and after simplification, we can get:

$$p_{PQ}(k,t)=\sum_{i=k}^{k_{max}}\binom{i-1}{i-k}(-1)^k e^{-\lambda t}\left(1-\sum_{r=0}^{i-1}X(r,\lambda((i-1)T_d-t))\right) \tag{B 5}$$

References

[1] B. Zhao, C. Wu, L. Sheng, Y. Liu, Next generation of space wireless communication technology based on X-ray, Acta Photonica Sin. 42 (2013) 801–804.

[2] S. Hang, X. Tang, H. Li, Y. Liu, J. Mu, W. Zhou, P. Dang, S. Lai, Potential application of X-ray communication in a Martian dust storm, Acta Astronaut. 166 (2020) 277–289.

[3] H. Li, X. Tang, S. Hang, Y. Liu, D. Chen, Potential application of X-ray communication through a plasma sheath encountered during spacecraft reentry into earth's atmosphere, J. Appl. Phys. 121 (2017) 123101.

[4] G. Porter, See Straight through Data Center Bandwidth Limitations with X-Rays, 2013.

[5] K. Gendreau, Pulsar navigation and X-ray communication demonstrations with the NICER payload on the ISS, in: 1st. Annual ISS Research and Development Conference, 2012.

[6] L. Keesey, NASA set to demonstrate X-ray communications in space. https://phys.org/news/2019-02-nasa-x-ray-space.html, 2019.

[7] J. Mu, X. Tang, Y. Liu, S. Lai, Z. Feng, W. Chen, Y. Wang, Design and performance test of pulse X-ray receiver based on LYSO-SiPM for X-ray communication, J. Lightwave Technol. (2022).

[8] TP Series SiPM -Model, JARY-TP3050-8×8C, TP3050 series SiPM datasheet, joinbon technology Co, Hubei, China (2024). Available at: https://www.joinbon.com/pro_other-22.html.

[9] P.A. Rodnyi, Physical Processes in Inorganic Scintillators, Crc Press Laser & Optical Science & Technology, 1997.

[10] M. Weber, Scintillation: mechanisms and new crystals, Nucl. Instrum. Methods Phys. Res. Sect. A Accel. Spectrom. Detect. Assoc. Equip. 527 (2004) 9–14.

[11] D. Renker, Geiger-mode avalanche photodiodes, history, properties and problems, Nucl. Instrum. Methods Phys. Res. Sect. A Accel. Spectrom. Detect. Assoc. Equip. 567 (2006) 48–56.

[12] P. Eraerds, M. Legré, A. Rochas, H. Zbinden, N. Gisin, SiPM for fast photon-counting and multiphoton detection, Opt Express 15 (2007) 14539–14549.

[13] Andrea Gallivanoni, Ivan Rech, Ghioni, Massimo, Progress in quenching circuits for single photon avalanche diodes, IEEE Trans. Nucl. Sci. 57 (2010) 3815–3826.

[14] E. Sarbazi, M. Safari, H. Haas, Statistical modeling of single-photon avalanche diode receivers for optical wireless communications, IEEE Trans. Commun. (2018) 1, 1.

[15] E. Sarbazi, M. Safari, H. Haas, The impact of long dead time on the photocount distribution of SPAD receivers, in: GLOBECOM 2018 - 2018 IEEE Global Communications Conference, 2018.

[16] S. Huang, S.M. Patanwala, J. Kosman, R.K. Henderson, M. Safari, Optimal photon counting receiver for sub-dead-time signal transmission, J. Lightwave Technol. (2020) 1, 1.

[17] H. Mahmoudi, M. Hofbauer, B. Steindl, K. Schneider-Hornstein, H. Zimmermann, Modeling and analysis of BER performance in a SPAD-based integrated fiber optical receiver, IEEE Photon. J. (2018) 1, 1.

[18] J. Du, Y. Wang, L. Zhang, Z. Zhou, X. Wang, Physical properties of LYSO scintillator for NN-pet detectors, in: International Conference on Biomedical Engineering & Informatics, 2009.

[19] C.C. Chen, Effect of Detector Dead Time on the Performance of Optical Direct-Detection Communication Links, the Telecommunications and Data Acquisition Report, 1988.

[20] E. Sarbazi, M. Safari, H. Haas, Photon detection characteristics and error performance of SPAD array optical receivers, in: 2015 4th International Workshop on Optical Wireless Communications (IWOW), 2015.

[21] B. Sklar, Digital Communications, Fundamentals and Applications, 1998.

[22] Z. Feng, Y. Liu, J. Mu, W. Chen, S. Lai, X. Tang, Optimization and testing of groove-shaped grid-controlled modulated X-ray tube for X-ray communication, Nucl. Instrum. Methods Phys. Res. (2022).